IEEE Access
Multidisciplinary | Rapid Review | Open Access Journal

Received 12 September 2023, accepted 23 September 2023, date of publication 26 October 2023, date of current version 6 November 2023.

Digital Object Identifier 10.1109/ACCESS.2023.3327920

RESEARCH ARTICLE

Block Adjustment of Orientation Parameters and Interferometric Parameters Using Very High-Resolution SAR Data for DSM Mapping

HAO ZHANG[1,2,3], GUOWANG JIN[1], XIN XIONG[1], JIN WANG[1], AND KAI GUAN[4]

[1]Institute of Geospatial Information, Information Engineering University, Zhengzhou 450001, China
[2]State Key Laboratory of Geo-Information Engineering, Xi'an 710001, China
[3]Xi'an Research Institute of Surveying and Mapping, Xi'an 710001, China
[4]Xi'an Surveying and Mapping Station, Xi'an 710054, China

Corresponding author: Guowang Jin (guowang_jin@163.com)

This work was supported in part by the National Natural Science Foundation of China under Grant 42201492.

ABSTRACT Block adjustment technology can effectively correct the interferometric parameter errors acquired from Interferometric Synthetic Aperture Radar (InSAR) system. It can reduce the number of required ground control points and improve the accuracy of the generated digital elevation model, making it's an effective means for obtaining three-dimensional information from large-scale terrain information. However, the currently used adjustment models usually only involve surface elevation parameters, which means that the accuracy of the terrain planimetric information entirely relies on the Position and Orientation System (POS) parameters. This may lead to the inaccurate planimetric to be a fundamental weakness which hinder the practical application of this technology. To solve these problems, this paper proposed a DSM (digital surface model) mapping scheme by using very high-resolution synthetic aperture radar (SAR) data that combines the block adjustments of orientation and interferometric parameters. Firstly, the interferometric and orientation parameters are obtained separately by using InSAR and SAR block adjustment techniques. After optimizing the model parameter accuracy, the elevation information obtained from the interferometric parameters is incorporated into the SAR positioning model to acquire the three-dimensional information of the area accurately. Experimental processing was conducted using 23 pairs of airborne InSAR data from two strips in the Weinan area of China. The experimental results demonstrate that the proposed scheme can improve the elevation accuracy by approximately 20%.

INDEX TERMS InSAR, block adjustment, orientation parameters, interferometric parameters.

I. INTRODUCTION

Synthetic aperture radar is an active microwave remote sensing sensor for Earth observation that can obtain high-precision images in all weather conditions and at all times [1]. It is often applied in research on volcanoes [2], [3], oceans [4], mines [5], forests [6], Etc. In contrast to optical sensors, SAR sensors perform two-dimensional range projections of terrain information to form images [7], [8]. In order to obtain three-dimensional terrain information, interferometric synthetic aperture radar technology is often used to process SAR images that satisfy coherence requirements. The technology generates interferometric phase information for elevation estimation within the coverage area of the images. When using SAR data for large-scale terrain mapping, a certain number of ground control points within the studied area are required in the InSAR process to ensure the accuracy of the extracted digital surface model (DSM). However, in actual mapping production, collecting a sufficient number of ground control points in the studied area is considerably costly.

Therefore, InSAR block adjustment methods are often used to reduce the dependence on ground control points [9]. A robust InSAR block adjustment scheme is crucial for

The associate editor coordinating the review of this manuscript and approving it for publication was Xuebo Zhang.

large-scale terrain extraction using SAR data. In the field of InSAR block adjustment, Farr et al. conducted the interferometric block adjustment research in Shuttle Radar Topography Mission (SRTM) [10], Prats-Iraola et al. derived the interferometric elevation sensitivity equation under slant view, determining the critical system parameters that need to be calibrated for interferometric parameter calibration [11]. With the TerraSAR mission system, Gruber et al. achieved processing results with a relative vertical error of fewer than 1.5 meters [12]. Yun et al. proposed a calibration method for airborne InSAR based on a reference DEM, which uses the reference Digital Elevation Model (DEM) to simulate SAR images and obtain control points for calibration [13]. Ma et al. proposed a method combining iterative approximation and LDL sparse matrix decomposition for optimization calculation [14] and a method for joint adjustment of InSAR images based on a Range Doppler (RD) model [15], [16], linearized with station coordinates and initial velocities was proposed successively. Jin et al. introduced the block adjustment method into InSAR interferometric parameter calibration using a dual-antenna airborne SAR system [17]. Lu et al. proposed a single-flight interferometric calibration method that simplifies traditional multi-flight interferometric calibration to single-flight calibration [18]. Gao et al. introduce the airborne dual-antenna Ka-band InSAR data processing method for typical terrains in China and proposes a robust and efficient method for phase unwrapping of interferometric data and strip adjustment calibration [19]. InSAR block adjustment technology can effectively refine interferometric parameters and support acquiring accurate terrain elevation information, but it cannot accurately obtain planimetric terrain information.

On the other hand, SAR image block adjustment can refine the orientation parameters through a small amount of control information and accurately intersect the three-dimensional information of terrain at the overlap of stereo images. Toutin et al. processed SAR images acquired by Radarsat-1 to obtain an adjustment result with an error of approximately 35 meters, verifying the effectiveness of image block adjustment in reducing the requirement for ground control points [20]. Yang et al. introduced Global Positioning System (GPS) and Inertial Measurement Unit (IMU) data into the adjustment and achieved good results [21]. Yue et al. proposed an adjustment method for airborne SAR images using the RD equation [22]. Ma et al. proposed a SAR image block adjustment method based on F.leberl's imaging model, inspired by the resection and intersection methods used in photogrammetry [23]. Yang et al. presented an airborne SAR image block adjustment method using trajectory constraint equations and the Schreiber rule [24]. Chang et al. proposed a robust UAV SAR image block adjustment method [25]. However, these techniques have a limited range for obtaining three-dimensional information and could be more conducive to efficient large-area terrain mapping production.

In order to solve the problems, this paper proposes a DSM mapping scheme using very high-resolution synthetic aperture radar data, which combines SAR image block adjustment and InSAR block adjustment methods. Due to the significant differences between the two adjustment models, directly combining them may lead to convergence difficulties or even non-convergence of the adjustment process. Therefore, in this work, we first use the InSAR block adjustment method to obtain terrain elevation information. Then, we incorporate the elevation information into the SAR image block adjustment model to extract three-dimensional terrain information accurately.

The subsequent structure of this paper is as follows. Section II explains the three-dimensional information extraction scheme using the combined adjustment of orientation parameters and interferometric parameters. In Section III, we mainly discuss the data used in the experiments, the results of block adjustment, and the accuracy comparison between the proposed scheme and the traditional elevation acquisition scheme which directly using POS data with the refined interferometric parameters. In Section IV, we give the meaningful results of the proposed scheme and possible further research directions in this field.

II. THREE-DIMENSIONAL TERRAIN INFORMATION EXTRACTION SCHEME

In the large-scale terrain three-dimensional information extraction using InSAR technology, the terrain plane information is generally obtained directly from the airborne POS data to complete the final DSM data production. However, both airborne systems and POS systems usually contain specific systematic errors, and directly using them may affect the accuracy of the generated DSM. Combining the SAR image block adjustment method makes it possible to obtain more accurate orientation parameters and improve the accuracy of the acquired terrain plane information. The specific process of combining two adjustment methods will be introduced first, followed by the introduction of the two adjustment methods separately.

A. DSM MAPPING THROUGH BLOCK ADJUSTMENTS OF ORIENTATION PARAMETERS AND INTERFEROMETRIC PARAMETERS

In current airborne SAR system applications, the initial parameters provided by the SAR system are usually not accurate enough for direct use. When used without refinement, they may have a particular impact on the final data generation accuracy. However, involving too many parameters in the calculations will significantly increase the computational difficulty of data processing methods like block adjustment. Considering all these factors and leveraging the relatively high accuracy of the velocity recording capability of the airborne POS system, this paper simplifies the original RD model by only using the initial three-dimensional coordinate positions of each image and the centroid frequency

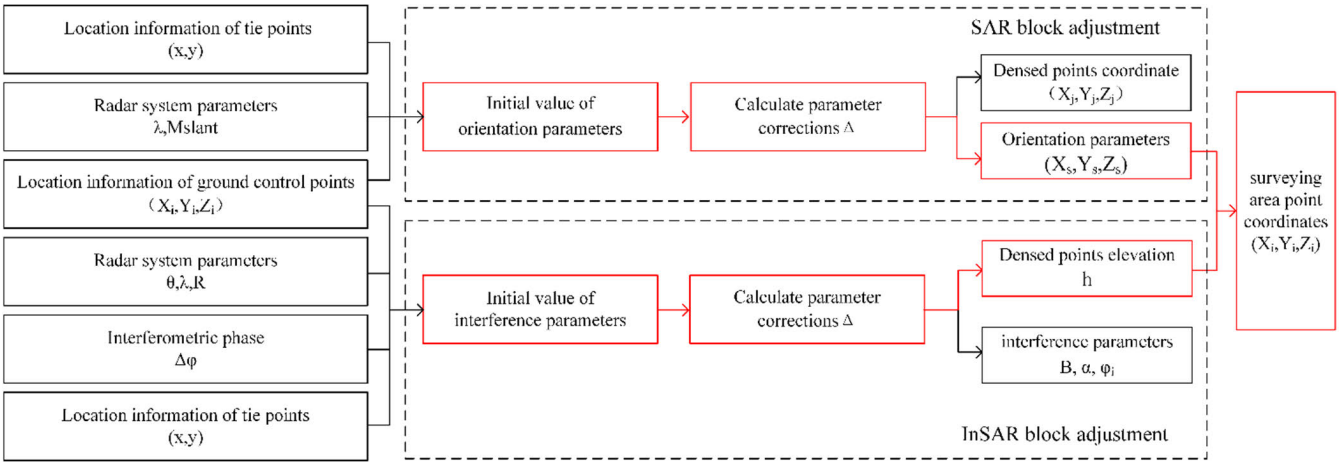

FIGURE 1. Flowchart of joint orientation parameters and interferometric parameters block adjustment scheme. The red portion represents the process of generating three-dimensional information.

of the Doppler as adjustment parameters. By doing this simplification, we can obtain a new error model.

In the specific data processing, based on the condition that any control point and tie point in the imaging area maintain consistent coordinate information after solving the coordinates through the RD model orientation parameter refinement, an RD model equation is formulated and solved iteratively through the least squares method with initial values for unknowns until the correction is smaller than the predetermined tolerance. This way, all orientation parameters and point position information for all SAR images in the survey area are obtained.

Similarly, based on the condition that any point in the imaging area satisfies the consistency of three-dimensional information after solving the InSAR height inversion model parameters, the linearized InSAR height equation with baseline length B, baseline angle α, interferometric phase bias ϕ_i, and point surface elevation h as unknowns is solved iteratively through the least squares method until the correction is smaller than the threshold, obtaining the interferometric parameters and point elevation data. Finally, the refined elevation information obtained through InSAR block adjustment is replaced with the RD model that has already obtained four orientation parameters to obtain the final surface three-dimensional information. The specific data processing flow is shown in Figure 1.

B. SAR IMAGE BLOCK ADJUSTMENT

This scheme primarily uses SAR block adjustment to obtain high-accuracy orientation parameters [9]. The imaging geometry of the SAR sensor is shown in Figure 2. Taking azimuth as the X-axis, with the positive direction along the flight direction of the carrier; taking range as the Y-axis, with the positive direction along the radar wave transmission direction; and the elevation image as the Z-axis. The three-axis velocity at the antenna phase center is defined as S_{X0}, S_{Y0}, and S_{Z0}. M_S is the slant range sampling interval

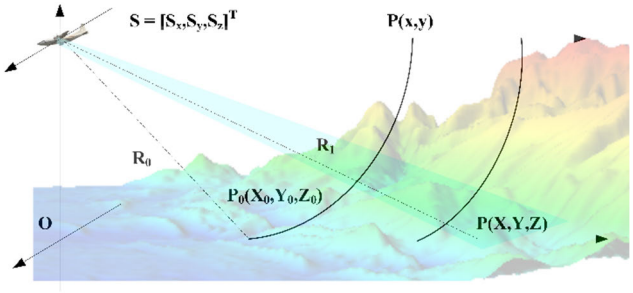

FIGURE 2. RD imaging model illustration.

of the SAR image. R_0 is the near-range delay. Assuming that the coordinates of a ground point are (X, Y, Z), and the corresponding coordinates on the image are (x, y), the transformation relationship between the physical and image coordinates can be established based on the simplified RD model, as shown in Equations (1) and (4).

$$\begin{aligned} R_s^2 &= (X - X_S)^2 + (Y - Y_S)^2 + (Z - Z_S)^2 \\ &= (R_0 + M_S \cdot y)^2 \end{aligned} \tag{1}$$

According to Equation (1), for a point $\boldsymbol{A_S} = [X_S\ Y_S\ Z_S]^{\mathrm{T}}$, we have $\boldsymbol{A_S} = \boldsymbol{A_{S0}} + \boldsymbol{S} \cdot t$, which can be written as Equation (2).

$$\begin{cases} X_S = X_{S0} + S_X t \\ Y_S = Y_{S0} + S_Y t \\ Z_S = Z_{S0} + S_Z t \\ t = t' \cdot x \end{cases} \tag{2}$$

During the imaging process, the velocity of the antenna phase center $\boldsymbol{S} = [S_X\ S_Y\ S_Z]^{\mathrm{T}}$ and slant range R_S satisfy Equation (3).

$$S_X(X - X_S) + S_Y(Y - Y_S) + S_Z(Z - Z_S) = -\frac{\lambda R_s}{2} f_{dc} \tag{3}$$

Based on the Equations (1) and (2), we have the following equation.

$$\begin{cases} \&F_1 = (X - X_S)^2 + (Y - Y_S)^2 + (Z - Z_S)^2 \\ \qquad - (R_S + M_S \cdot x)^2 \\ \&F_2 = S_X (X - X_S) + S_Y (Y - Y_S) + S_Z (Z - Z_S) \\ \qquad + \dfrac{\lambda (R_S + M_S \cdot x)}{2} f_{dc} \end{cases} \tag{4}$$

If we do not consider the correction of the image point coordinates, the linearized range-Doppler model can be represented as:

$$\boldsymbol{A} \cdot \boldsymbol{\Delta}_O + \boldsymbol{C} \cdot \boldsymbol{\Delta}_G - \boldsymbol{L} = 0 \tag{5}$$

Among them, $\boldsymbol{\Delta}_{\mathrm{O}}$ is the correction vector for orientation parameters; $\mathbf{A}$ is the coefficient matrix, $\boldsymbol{\Delta}_{\mathrm{G}}$ is the correction vector for ground point coordinates, $\mathbf{C}$ is the coefficient matrix, and $\mathbf{L}$ is the constant term. In each SAR image, with the initial values of 4 orientation parameters being X_{S0}, Y_{S0}, $Z_{\mathrm{S0}}, f_{\mathrm{dc}}$:

$$\mathbf{A} = \begin{bmatrix} a_{10} & a_{11} & a_{12} & a_{13} \\ a_{20} & a_{21} & a_{22} & a_{23} \end{bmatrix} \tag{6}$$

$$\begin{cases} a_{10} = \dfrac{\partial F_1}{\partial X_{S0}} = -2(X - X_S) \\ a_{11} = \dfrac{\partial F_1}{\partial Y_{S0}} = -2(Y - Y_S) \\ a_{12} = \dfrac{\partial F_1}{\partial Z_{S0}} = -2(Z - Z_S) \\ a_{13} = \dfrac{\partial F_1}{\partial f_{dc}} = 0 \end{cases} \quad \begin{cases} a_{20} = \dfrac{\partial F_2}{\partial X_{S0}} = -S_X \\ a_{21} = \dfrac{\partial F_2}{\partial Y_{S0}} = -S_Y \\ a_{22} = \dfrac{\partial F_2}{\partial Z_{S0}} = -S_Z \\ a_{23} = \dfrac{\partial F_2}{\partial f_{dc}} \\ \quad = \dfrac{\lambda (R_S + M_S \cdot y)}{2} \end{cases} \tag{7}$$

$$\boldsymbol{\Delta}_O = \begin{bmatrix} \Delta X_{S0} & \Delta Y_{S0} & \Delta Z_{S0} & \Delta f_{dc} \end{bmatrix}^T \tag{8}$$

$$\boldsymbol{C} = \begin{bmatrix} c_{10} & c_{11} & c_{12} \\ c_{20} & c_{21} & c_{22} \end{bmatrix} \tag{9}$$

$$\begin{cases} c_{10} = \dfrac{\partial F_1}{\partial X} = 2(X - X_S) \\ c_{11} = \dfrac{\partial F_1}{\partial Y} = 2(Y - Y_S) \\ c_{12} = \dfrac{\partial F_1}{\partial Z} = 2(Z - Z_S) \end{cases} \quad \begin{cases} c_{20} = \dfrac{\partial F_2}{\partial X} = S_X \\ c_{21} = \dfrac{\partial F_2}{\partial Y} = S_Y \\ c_{22} = \dfrac{\partial F_2}{\partial Z} = S_Z \end{cases} \tag{10}$$

$$\boldsymbol{\Delta}_G = \begin{bmatrix} \Delta X & \Delta Y & \Delta Z \end{bmatrix}^T \tag{11}$$

$$\boldsymbol{L} = \begin{bmatrix} F_1^0 & F_2^0 \end{bmatrix}^T \tag{12}$$

$$\begin{cases} F_1^0 = (X^0 - X_S^0)^2 + (Y^0 - Y_S^0)^2 + (Z^0 - Z_S^0)^2 \\ \qquad -(R_S + M_S \cdot y)^2 \\ F_2^0 = S_X (X^0 - X_S^0) + S_Y (Y^0 - Y_S^0) + S_Z (Z^0 - Z_S^0) \\ \qquad + \dfrac{\lambda f_{dc}^0}{2} (R_S + M_S \cdot y) \end{cases} \tag{13}$$

where the superscript ^{0} symbol represents the initial value of the parameter. Based on the linearized expression of the RD model shown in Equation (1), a set of error equations can be established for each control point and tie point in the image. Assuming InSAR images are in the region block, the i-th image has $\mathrm{m_i}$ control points and $\mathrm{n_i}$ tie points. Therefore, the correction vector for the orientation parameters corresponding to the i-th SAR image is:

$$\boldsymbol{\Delta}_O^i = \begin{bmatrix} \Delta X_{S0}^i & \Delta Y_{S0}^i & \Delta Z_{S0}^i & \Delta f_{dc}^i \end{bmatrix}^T \tag{14}$$

Let $\mathrm{im_j}$ denote the j-th control point in the i-th SAR image, $\mathrm{A^{im_j}}$ represents the coefficient matrix for the corresponding correction vector of the orientation parameters, $\mathrm{L^{im_j}}$ represents the constant term, and $\mathrm{p^{im_j}}$ represents the weight of the corresponding error equation. If the ground coordinates of the control points are considered actual values, the original error equation can be obtained as:

$$\boldsymbol{v}^{im_j} = \boldsymbol{A}^{im_j} \cdot \boldsymbol{\Delta}_P^i - \boldsymbol{L}^{im_j} \boldsymbol{p}^{im_j} \tag{15}$$

For tie points, assuming $\mathrm{in_j}$ represents the j-th tie point in the i-th image, $\boldsymbol{A}^{\mathrm{in_j}}$ represents the coefficient matrix for the correction vector of the orientation parameters at that point, $\boldsymbol{L}^{\mathrm{in_j}}$ represents the constant term, and $\boldsymbol{p}^{\mathrm{in_j}}$ represents the weight of the error equation constructed based on the RD model. Then, the original error equation can be represented as:

$$\boldsymbol{v}^{in_j} = \boldsymbol{A}^{in_j} \cdot \boldsymbol{\Delta}_P^i + \boldsymbol{C}^{in_j} \cdot \boldsymbol{\Delta}_G^{in_j} - \boldsymbol{L}^{in_j} \boldsymbol{p}^{in_j} \tag{16}$$

The weight $\boldsymbol{p}$ can be expressed as:

$$\boldsymbol{p} = \begin{bmatrix} p_1 & \\ & p_2 \end{bmatrix} \tag{17}$$

All control points and tie points can be used to form a set of error equations according to equations (16) and (17), which constitute an error equation system. The least squares method is employed to adjust and solve each unknown globally.

C. INSAR BLOCK ADJUSTMENT

In this scheme, InSAR block adjustment is primarily used to obtain large-scale elevation information [26]. The coordinate system is defined similarly to the RD imaging model mentioned above. As shown in Figure 3, let the elevation of the ground point P be h, the elevation of the radar antenna center $\mathrm{A_1}$ be H, the viewing angle at the observation time be θ, the baseline length between the master and slave antennas be B, the angle between the horizontal direction and the baseline be α, R and R' be the slant range differences between the ground point P and the phase centers of the master and slave antennas, respectively. ΔR is the difference in slant range between the two image centers and the ground point P ($\Delta \mathrm{R} = R' - R$).

Let β be the angle between baseline $\mathrm{A_1A_2}$ and $\mathrm{A_1P}$. Then, in triangle $\mathrm{A_1A_2P}$, we have:

$$\cos\beta = \frac{R^2 + B_{\mathrm{L}}^2 - R'^2}{2RB_{\mathrm{L}}} = \frac{R^2 + B_{\mathrm{L}}^2 - (R + \Delta \mathrm{R})^2}{2RB_{\mathrm{L}}}$$

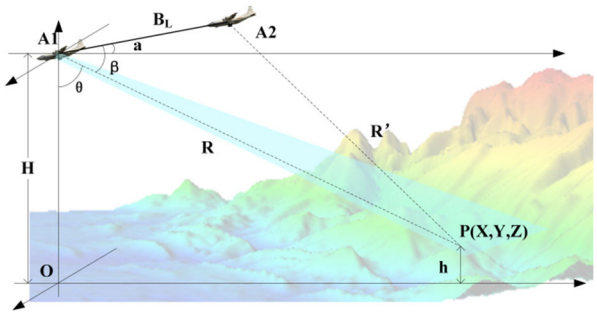

FIGURE 3. InSAR geometric model illustration.

$$= -\frac{\Delta R}{B_L} + \frac{B_L}{2R} - \frac{\Delta R^2}{2RB_L} \tag{18}$$

Therefore, according to the triangle relationships shown in the figure, the corresponding elevation measurement can be expressed as:

$$B_L \sin(\theta - \alpha) + \Delta R - \frac{B_L^2}{2R} + \frac{\Delta R^2}{2R} = 0 \tag{19}$$

where λ represents the wavelength, φ_0 represents the interferometric phase bias, and $\Delta\varphi$ represents the unwrapped interferometric phase. Based on the spatial imaging relationship, we can obtain:

$$\Delta R = \frac{\varphi_0 + \Delta\varphi}{2\pi}\lambda \tag{20}$$

Then Equation (17) can be represented as a nonlinear equation of ϕ_0, B_L, α, and h:

$$F(B_L, \alpha, \varphi_0, h) = 0 \tag{21}$$

Linearizing this equation, the corresponding error equation is:

$$v = b_0\Delta B_L + b_1\Delta\alpha + b_2\Delta\phi_0 + b_3\Delta h - l \tag{22}$$

where v represents the error, ΔB_L, $\Delta\alpha$, $\Delta\phi_0$, and Δh are the correction terms for their respective parameters, b_0, b_1, b_2 and b_3 are the coefficients associated with the correction terms, and l is the constant term.

Expressing equation (23) in matrix form:

$$\boldsymbol{V} = [\boldsymbol{A} \quad \boldsymbol{B}]\begin{bmatrix}\boldsymbol{\Delta}_I \\ \boldsymbol{\Delta}_G\end{bmatrix} - \boldsymbol{L} \tag{23}$$

while

$$\boldsymbol{V} = [v] \tag{24}$$
$$\boldsymbol{A} = \begin{bmatrix} b_0 & b_1 & b_2 \end{bmatrix} \tag{25}$$
$$\boldsymbol{B} = [b_3] \tag{26}$$
$$\boldsymbol{\Delta}_I = \begin{bmatrix}\Delta B_L & \Delta\alpha & \Delta\varphi_0\end{bmatrix}^T \tag{27}$$
$$\boldsymbol{\Delta}_G = [\Delta h] \tag{28}$$
$$\boldsymbol{L} = [l] \tag{29}$$

For the dual-baseline InSAR configuration, the corresponding coefficients of the unknowns can be expressed as:

$$\begin{cases} b_0 = \dfrac{\partial F}{\partial B} = \sin(\arccos\dfrac{H-h}{R} - \alpha) - \dfrac{B_L}{R} \\ b_1 = \dfrac{\partial F}{\partial \alpha} = -B_L\cos(\arccos\dfrac{H-h}{R} - \alpha) \\ b_2 = \dfrac{\partial F}{\partial \varphi_0} = -\dfrac{\lambda}{2\pi} - \dfrac{\Delta R}{R}\dfrac{\lambda}{2\pi} \\ b_3 = \dfrac{\partial F}{\partial h} = \dfrac{1}{\sqrt{R^2-(H-h)^2}}B_L\cos(\arccos\dfrac{H-h}{R} - \alpha) \end{cases} \tag{30}$$

While l is

$$l = -B_{L0}\sin(\arccos\frac{H-h}{R} - \alpha_0) - \Delta R + \frac{B_{L0}^2}{2R} - \frac{\Delta R^2}{2R} \tag{31}$$

When processing the images, the ground control points can participate in the solution as shown in the following equation:

$$v_{GCP1} = F(B_{L1}, \alpha_1, \phi_{10}) \tag{32}$$

For tie points, the corresponding equations can be constructed based on their respective positions.

$$v_{TP2} = F(B_{L2}, \alpha_1, \phi_{10}, h_{TP2}) \tag{33}$$

Similarly, for all control points and tie points, error equations are constructed. By iteratively solving these equations, the interferometric parameters and tie point elevations can be determined. This approach effectively reduces the number of required ground control points.

To improve the performance of the adjustment solution, this work adopts the InSAR block adjustment method utilizing the Schreiber rule to construct equivalent error equations. Combining the aforementioned method, the error equation for the corresponding elevation control points is given by Equation (34).

$$\boldsymbol{V} = \boldsymbol{A}\boldsymbol{\Delta}_I - \boldsymbol{L} \quad \boldsymbol{P} \tag{34}$$

The error equation for the densed point is as follows:

$$\boldsymbol{V} = \boldsymbol{A}\cdot\boldsymbol{\Delta}_I + \boldsymbol{C}\cdot\boldsymbol{\Delta}_G - \boldsymbol{L} \quad \boldsymbol{P} \tag{35}$$

If the elevation densed point i falls within the N-degree overlap range of the InSAR interferometric image pair, its equivalent error equation group can be expressed as:

$$\begin{cases} \boldsymbol{V}' = \boldsymbol{A}_j\boldsymbol{\Delta}_{Ij} - \boldsymbol{L}_j \quad j = 1, 2, \cdots, N \qquad \boldsymbol{P}_{ij} \\ \boldsymbol{V}_0 = \sum_{j=1}^{N}\left(\boldsymbol{C}_j^T\boldsymbol{P}_j\boldsymbol{A}_j\boldsymbol{\Delta}_{Ij}\right) - \sum_{j=1}^{N}\left(\boldsymbol{C}_j^T\boldsymbol{P}_j\boldsymbol{L}_j\right) \\ \qquad\qquad - \sum_{j=1}^{N}\left(\boldsymbol{C}_j^T\boldsymbol{P}_j\boldsymbol{C}_j\right)^{-1} \end{cases} \tag{36}$$

Based on this, the error equations can be derived for all elevation control points and elevation densed points.

FIGURE 4. Overview of the studied area.

TABLE 1. InSAR system parameter information table.

Parameter type	Parameter value
Wavelength (m)	0.008565
Radar Frequency (GHz)	35
Azimuth Sampling Interval (m)	0.120
Range Sampling Interval (m)	0.134
Near Range Delay (m)	3599.5
Absolute Orbit Altitude (m)	3434.7

During the computation, with the given initial values of interferometric parameters, the correction quantities for the interferometric parameters are solved by solving the equivalent error equation system. The initial values are adjusted iteratively until all correction quantities meet the required tolerance conditions. After obtaining the adjustment values for all interferometric image pairs, the corresponding phase unwrapping results are searched at each densed point to obtain the elevation [27].

III. EXPERIMENTS

A. EXPERIMENTAL DATA

The experimental data is obtained from an airborne, high-resolution millimeter-wave InSAR system from the 23rd Institute of China Aerospace Science and Industry Corporation. DSM mapping experiments were conducted based on the acquired data, and the studied area is shown in Figure 4. The flight direction of the aircraft was from west to east, and two flight lines were acquired, labeled as ''1001'' and ''1052,'' each containing 12 InSAR interferometric pairs with suffix numbers from ''002'' to ''013.'' Due to a system failure, the ''1052'' flight line failed to acquire data for pair ''005.'' Each interferometric pair covers an area of approximately 1.75 km by 1.5 km, and the entire studied area is 17.5 km by 2.5 km. Some parameters of the InSAR system are shown in Table 1.

The western side of the studied area is hilly terrain with apparent undulations, followed by a relatively flat plain area with extensive farmland and a few residential areas. There is a deep ravine on the eastern side of the studied area, dividing the eastern plain area into two parts. The highest point in the studied area is located in the hilly area on the west side, with an elevation of approximately 680 meters. In contrast, the lowest point is located in the ravine on the east side, with an elevation of approximately 390 meters. Although the overall range of the studied area is not a very big regional terrain. However, the surveyed area includes major terrains such as hills, plains, and gullies in relatively flat areas, which can

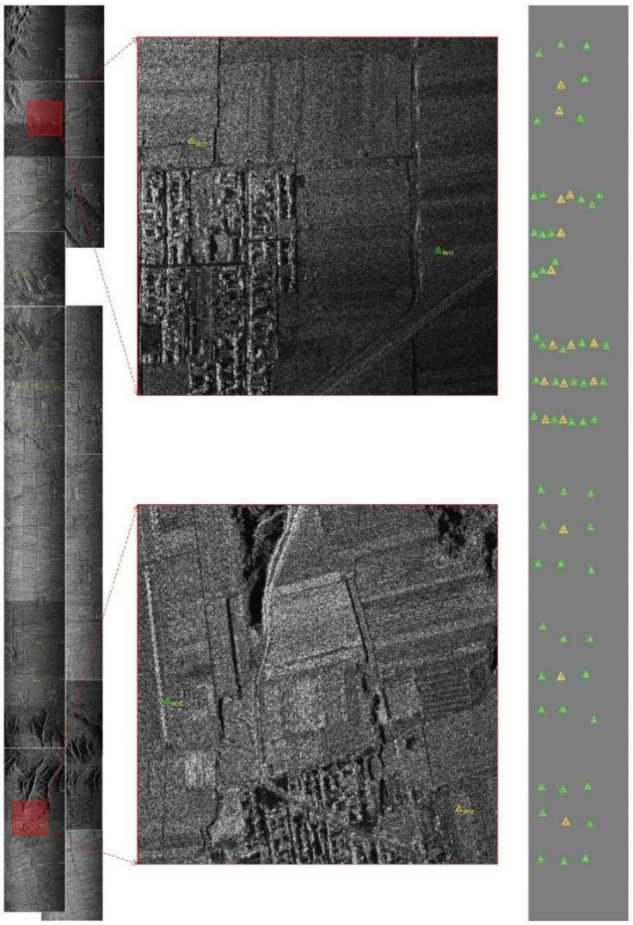

FIGURE 5. Distribution of control points(green triangle) and check points(yellow triangle). The zoomed-in portion of the image corresponds to the data indicated by the red box on the left.

effectively verify the reliability of the proposed approach in this paper. Furthermore, the differentiated adjustment results in different types of regions can also serve as a reflection of the effectiveness of applying this approach to specific regions.

The parameters involved in the SAR block adjustment calculation include the coordinates of tie points and ground control points, as well as variables such as wavelength, sampling interval, station coordinates, and Doppler center frequency. On the other hand, the parameters involved in the InSAR block adjustment calculation include the interferometric phase, coordinates of tie points, and radar system parameters such as wavelength and slant range. The ground control points and checkpoints were obtained through RTK (Real-time kinematic) measurements and then transformed into a Gauss-Plane coordinate system. Seventy-two ground points were measured within the studied area, including 18 checkpoints and 56 ground control points. Figure 5 shows the distribution of checkpoints and control points in the studied area, with control points represented by green triangle markers and checkpoints represented by yellow triangle markers. The improved SAR-SIFT algorithm [28]

TABLE 2. Orientation parameter estimation results of SAR image block adjustment.

Image Name	Initial Position (m)			Doppler Centroid Frequency (Hz)
	X_{S_0}	Y_{S_0}	Z_{S_0}	
1001_002	**88493.704	**408682.114	3433.754	-177.481
1001_003	**88483.830	**410106.781	3433.836	-190.742
1001_004	**88473.461	**411532.155	3433.943	-207.971
1001_005	**88461.753	**412958.051	3434.032	-233.806
1001_006	**88447.135	**414382.167	3434.098	-238.152
1001_007	**88432.918	**415807.329	3433.826	-219.210
1001_008	**88421.391	**417231.426	3433.824	-234.537
1001_009	**88407.850	**418655.336	3434.352	-239.859
1001_010	**88394.331	**420079.729	3434.423	-228.312
1001_011	**88382.339	**421504.271	3434.390	-229.401
1001_012	**88370.653	**422928.973	3434.166	-215.297
1001_013	**88360.610	**424352.999	3433.961	-204.619
1052_002	**87586.731	**408602.666	3433.857	-444.092
1052_003	**87585.852	**410095.689	3433.618	-186.203
1052_004	**87579.065	**411523.675	3433.843	-210.364
1052_006	**87554.971	**414373.747	3433.924	-227.890
1052_007	**87543.402	**415797.988	3433.775	-253.457
1052_008	**87528.780	**417218.419	3434.166	-278.905
1052_009	**87512.926	**418677.954	3434.269	-90.704
1052_010	**87500.770	**420081.509	3434.012	-167.672
1052_011	**87490.974	**421492.006	3433.917	-239.223
1052_012	**87480.018	**422910.875	3434.147	-286.571
1052_013	**87466.086	**424343.843	3434.170	-242.396

was used to extract tie points required for adjustment in the overlapping areas.

B. BLOCK ADJUSTMENT RESULTS

1) SAR IMAGE BLOCK ADJUSTMENT RESULTS

After the block adjustment of SAR images, the results of solving the orientation parameters for the 23 SAR images (including initial position parameters of the radar antenna and Doppler centroid frequency) are shown in Table 2. Table 3 and Figure 6 show the statistical results of the SAR image block adjustment accuracy.

According to Table 3, the maximum error in the X direction of the SAR image block adjustment is 0.215 meters, the minimum error is 0.006 meters, and the RMSE is 0.088 meters. The maximum error in the Y direction is 0.157 meters, the minimum error is 0.005 meters, and the RMSE is 0.055 meters. The maximum error in the Z direction is 0.236 meters, the minimum error is 0.017 meters, and the RMSE is 0.089 meters

According to Figure 6 there is no apparent systematic error in all three directions, indicating the correctness and effectiveness of the block adjustment model for the SAR image area.

TABLE 3. Check point errors of SAR image block adjustment.

Point ID	Check Point Error		
	X Direction (m)	Y Direction (m)	Z Direction (m)
B021	-0.016	-0.005	-0.017
B023	-0.084	0.078	-0.066
B032	-0.097	-0.056	-0.083
B512	-0.215	-0.039	-0.192
B523	-0.071	0.007	-0.077
B641	0.025	-0.036	0.05
B651	0.213	-0.03	0.236
B652	0.129	-0.026	0.142
B663	0.134	0.142	0.135
B721	0.099	0.157	0.096
B722	0.133	-0.037	0.132
B741	0.006	0.026	0.023
B752	0.026	-0.034	0.027
B761	0.061	0.052	0.06
B772	-0.153	-0.041	-0.138
B773	-0.049	0.071	-0.044
B822	0.052	0.069	0.054
B922	0.028	-0.081	0.03
Max	0.215	0.157	0.236
Min	0.006	0.005	0.017
RMSE	0.088	0.055	0.089

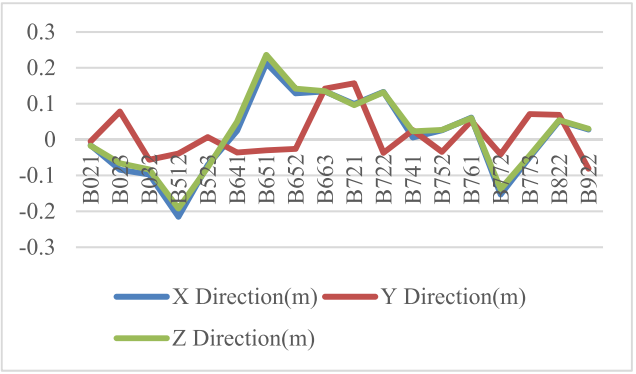

FIGURE 6. Check point errors of SAR image block adjustment.

2) INSAR BLOCK ADJUSTMENT RESULTS

After the block adjustment of InSAR data, the results of solving the interferometric parameters (including interferometric phase bias, baseline length, and baseline azimuth) for the 23 sets of InSAR image pairs are shown in Table 4.

The statistical results of the accuracy of the InSAR block adjustment are shown in Table 5 and Figure 7. According to Table 5, the maximum height error of the block adjustment method is 2.399 meters, the minimum error is 0.017 meters, and the RMSE is 0.654 meters. As shown in Figure 7, there is no apparent systematic error in the height direction, indicating the correctness and effectiveness of the InSAR block adjustment model.

TABLE 4. Interferometric parameter estimation results of InSAR block adjustment.

Image Name	Baseline Length B	Baseline Horizontal Angle α	Interferometric Phase Offset ϕ0
1001_002	0.119	0.564	-21.024
1001_003	0.117	0.659	-13.938
1001_004	0.116	0.773	0.825
1001_005	0.118	0.630	-18.152
1001_006	0.123	0.477	-25.174
1001_007	0.122	0.499	-21.572
1001_008	0.122	0.505	-20.105
1001_009	0.122	0.500	-20.388
1001_010	0.126	0.403	-29.712
1001_011	0.128	0.365	-39.808
1001_012	0.129	0.355	-37.471
1001_013	0.126	0.404	-29.874
1052_002	0.119	0.581	-15.644
1052_003	0.117	0.646	-9.904
1052_004	0.119	0.579	-22.013
1052_006	0.124	0.436	-27.287
1052_007	0.124	0.451	-25.004
1052_008	0.120	0.544	-22.084
1052_009	0.119	0.606	-10.598
1052_010	0.119	0.630	-8.447
1052_011	0.119	0.641	-7.763
1052_012	0.121	0.542	-18.227
1052_013	0.119	0.582	-18.862

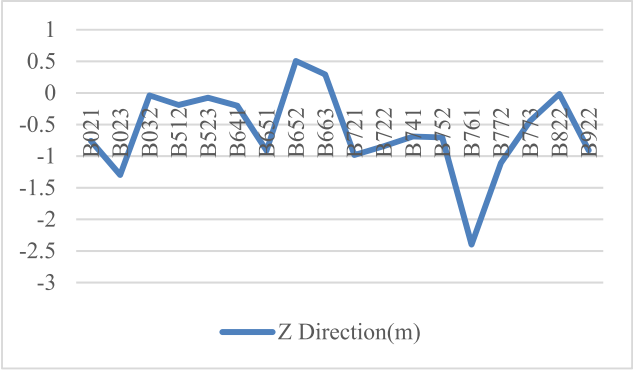

FIGURE 7. Check point errors of InSAR block adjustment.

According to Figure 7, there is no apparent systematic error in the elevation direction, indicating the correctness and effectiveness of the block adjustment model for the InSAR area.

C. DSM GENERATION

After obtaining the three-dimensional ground information, subsequent encoding, DSM filtering, and stitching were performed. The multi-level moving surface fitting filtering algorithm [29] was used for filtering, and the processed data results are shown in Figures 8, 9, and 10.

TABLE 5. Check point errors of InSAR block adjustment.

Point ID	Elevation Measurement	Calculated Elevation	Elevation Error /Z Direction(m)
B021	541.193	540.435	-0.758
B023	538.412	537.115	-1.297
B032	548.814	548.775	-0.039
B512	625.632	625.441	-0.191
B523	629.137	629.061	-0.076
B641	635.634	635.431	-0.203
B651	639.436	638.524	-0.912
B652	648.899	649.405	0.506
B663	653.617	653.909	0.292
B721	548.612	547.629	-0.983
B722	536.579	535.735	-0.844
B741	562.92	562.23	-0.69
B752	555.323	554.62	-0.703
B761	585.402	583.003	-2.399
B772	579.671	578.563	-1.108
B773	557.644	557.2	-0.444
B822	544.363	544.346	-0.017
B922	541.486	540.578	-0.908
Maximum value			2.399
Minimum value			0.017
RMSE			0.654

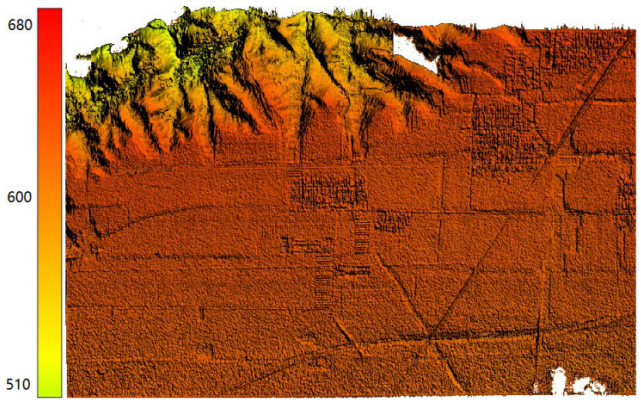

FIGURE 8. Illustration of results in the eastern hilly area.

D. ACCURACY COMPARISON AND ANALYSIS

To verify the effectiveness of the proposed combined adjustment method for SAR orientation parameters and InSAR interferometric parameters in obtaining surface three-dimensional information, the same control point data was used to compare the elevation accuracy between this proposed method and the individual InSAR block adjustment method [30]. The orientation parameters and interferometric parameters used in the experiment were obtained from the

TABLE 6. Comparison of InSAR block adjustment with elevation estimation results from this work.

Serial Number	ID	Elevation Measurement	Elevation Acquired from the Individual InSAR Block Adjustment Method	Elevation Acquired from this Work	Error from Individual InSAR Block Adjustment Method	Error from this Work
1	B021	541.193	540.8	540.435	-0.393	-0.758
2	B023	538.412	537.159	537.115	-1.253	-1.297
3	B032	548.814	548.805	548.775	-0.009	-0.039
4	B512	625.632	625.836	625.441	0.204	-0.191
5	B523	629.137	628.551	629.061	-0.586	-0.076
6	B641	635.634	634.111	635.431	-1.523	-0.203
7	B651	639.436	638.002	638.524	-1.434	-0.912
8	B652	648.899	648.912	649.405	0.013	0.506
9	B663	653.617	653.69	653.909	0.073	0.292
10	B721	548.612	547.329	547.629	-1.283	-0.983
11	B722	536.579	535.73	535.735	-0.849	-0.844
12	B741	562.92	562.329	562.23	-0.591	-0.69
13	B752	555.323	554.276	554.62	-1.047	-0.703
14	B761	585.402	582.298	583.003	-3.104	-2.399
15	B772	579.671	578.229	578.563	-1.442	-1.108
16	B773	557.644	556.738	557.2	-0.906	-0.444
17	B822	544.363	544.597	544.346	0.234	-0.017
18	B922	541.486	540.597	540.578	-0.889	-0.908

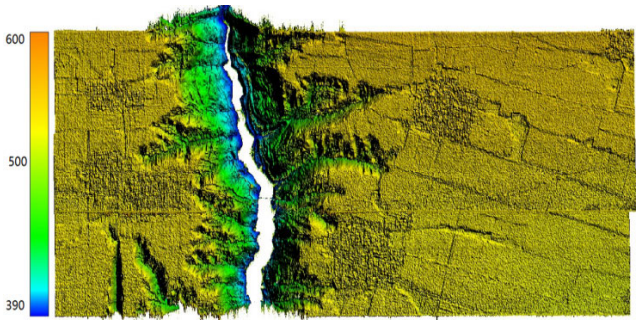

FIGURE 9. Illustration of results in the western plain area.

FIGURE 10. Filtered DSM result.

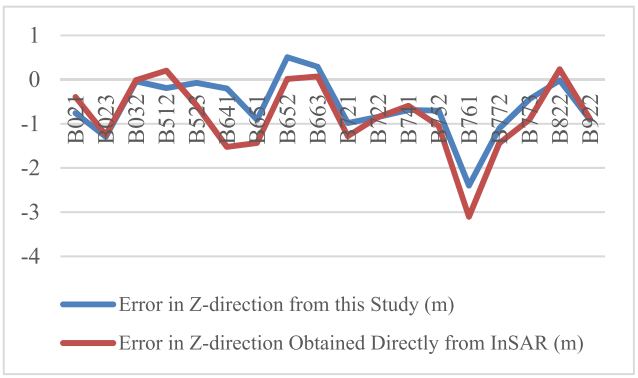

FIGURE 11. Comparison of elevation errors between the proposed method in this work and the individual InSAR block adjustment method only using InSAR block adjustment method for check point.

POS system and InSAR system on the plane. It should be noted that, unlike the conventional approach used for comparison, the station positions' coordinate and the center frequency used in the individual InSAR block adjustment method were not corrected through SAR block adjustment. After the adjustment process. The accuracy results are shown in Table 6, and the comparison results are shown in Figure 11.

Statistical analysis shows that the proposed approach in this paper effectively improves the elevation accuracy of the final results. The maximum elevation error of the proposed method is 2.399 meters, the minimum of it is 0.017 meters, and the RMSE of it is 0.654 meters. Using only the InSAR block adjustment method directly, the maximum elevation error is 3.104 meters, the minimum one is 0.009 meters, and the RMSE of it is 0.801 meters. In terms of the RMSE of the elevation data the proposed method achieves an improvement of about 20% in elevation accuracy.

To analyze the positioning accuracy enhancement ability of the proposed approach, all checkpoints were examined, and all points with elevation accuracy below 1 meter in any approach were extracted for analysis. This includes the four points (B023, B641, B772, B752) at the intersection of two image pairs and the three points (B721, B651, B761) on single image pairs. The precision statistics and point distribution are shown in the table below.

TABLE 7. Optimization of point accuracy situation.

Point ID	B023	B641	B651	B721	B752	B761	B772
Error of the Individual InSAR Block Adjustment	-1.253	-1.523	-1.434	-1.283	-1.047	-3.104	-1.442
Error from this work	-1.297	-0.203	-0.912	-0.983	-0.703	-2.399	-1.108
Difference in percentage	103.51%	13.33%	63.60%	76.62%	67.14%	77.29%	76.84%

From the comparison of elevation accuracy results, it can be observed that the proposed approach effectively improves the elevation information accuracy in areas with relatively abundant control information. Except for point B023 mentioned earlier, the average error of the other six points decreased by 62.47% compared to the previous error. However, for point B023, which has less surrounding control information, there was little change in accuracy.

IV. CONCLUSION

In this paper, a DSM mapping scheme combining SAR orientation parameter block adjustment and InSAR interferometric parameter block adjustment is designed. The proposed scheme was applied to extracting three-dimensional terrain information using the interferometric data obtained by the airborne very high-resolution millimeter-wave InSAR system. After verifying the correctness of the adjustment results for both the orientation parameters and interferometric parameters with GCPs, the DSM data of the image coverage area was obtained through geocoding. Furthermore, in order to compare the accuracy improvements between the proposed scheme and the traditional scheme which generating the terrain information directly from POS data, the studied area's DSM data were generated by using both schemes. Based on the acquired data, it was found that the proposed scheme achieved about 20% improvement in elevation accuracy compared to the traditional InSAR block adjustment scheme.

The SAR block adjustment and InSAR block adjustment methods are only result-driven and integrated into the proposed scheme. Our future work will explore schemes for deeply integrating the two adjustment methods and analyze the impacts of the number and distribution of ground control points on adjustment accuracy.

REFERENCES

[1] J. L. Mesa-Mingorance and F. J. Ariza-López, "Accuracy assessment of digital elevation models (DEMs): A critical review of practices of the past three decades," *Remote Sens.*, vol. 12, no. 16, p. 2630, Aug. 2020.

[2] M. J. W. Bemelmans, J. Biggs, M. Poland, J. Wookey, S. K. Ebmeier, A. K. Diefenbach, and D. Syahbana, "High-resolution InSAR reveals localized pre-eruptive deformation inside the Crater of Agung volcano, Indonesia," *J. Geophys. Res., Solid Earth*, vol. 128, no. 5, May 2023, Art. no. e2022JB025669.

[3] M. Angarita, R. Grapenthin, S. Plank, F. J. Meyer, and H. Dietterich, "Quantifying large-scale surface change using SAR amplitude images: Crater morphology changes during the 2019–2020 shishaldin volcano eruption," *J. Geophys. Res., Solid Earth*, vol. 127, no. 8, Aug. 2022, Art. no. e2022JB024344.

[4] A. G. Voronovich and V. U. Zavorotny, "Measurement of ocean wave directional spectra using airborne HF/VHF synthetic aperture radar: A theoretical evaluation," *IEEE Trans. Geosci. Remote Sens.*, vol. 55, no. 6, pp. 3169–3176, Jun. 2017.

[5] F. A. Temporim, F. F. Gama, W. R. Paradella, J. C. Mura, G. G. Silva, and A. R. Santos, "Spatiotemporal monitoring of surface motions using DInSAR techniques integrated with geological information: A case study of an iron mine in the Amazon region using TerraSAR-X and RADARSAT-2 data," *Environ. Earth Sci.*, vol. 77, no. 19, p. 688, Oct. 2018.

[6] M. Liu, C. Cao, Y. Dang, and X. Ni, "Mapping forest canopy height in mountainous areas using ZiYuan-3 stereo images and Landsat data," *Forests*, vol. 10, no. 2, p. 105, Jan. 2019.

[7] F. W. Leberl, M. Millot, R. S. Wilson, M. Karspeck, B. Mercer, and S. Thornton, "Radargrammetric image processing with a softcopy stereo workstation," in *Proc. 8th Thematic Conf. Geologic Remote Sens.*, vol. 8, 1991, pp. 639–647.

[8] F. Bovenga, "Special issue 'synthetic aperture radar (SAR) techniques and applications,'" *Sensors*, vol. 20, no. 7, p. 1851, Mar. 2020.

[9] X. Xiong, G. Jin, Q. Xu, and H. Zhang, "Block adjustment with airbrone SAR very high-resolution images using trajectory constraints," *Int. J. Remote Sens.*, vol. 39, no. 8, pp. 2383–2398, Apr. 2018.

[10] T. G. Farr, P. A. Rosen, E. Caro, R. Crippen, R. Duren, S. Hensley, M. Kobrick, M. Paller, E. Rodriguez, L. Roth, D. Seal, S. Shaffer, J. Shimada, J. Umland, M. Werner, M. Oskin, D. Burbank, and D. Alsdorf, "The shuttle radar topography mission," *Rev. Geophys.*, vol. 45, no. 2, p. 361, Jun. 2007.

[11] P. Prats, J. J. Mallorqui, and A. Broquetas, "Calibration of interferometric airborne SAR images using a multisquint processing approach," in *Proc. IEEE Int. Geosci. Remote Sens. Symp.*, Jul. 2003, pp. 4353–4355.

[12] A. Gruber, B. Wessel, M. Huber, and A. Roth, "Operational TanDEM-X DEM calibration and first validation results," *ISPRS J. Photogramm. Remote Sens.*, vol. 73, pp. 39–49, Sep. 2012.

[13] Y. Yun, Q. Zeng, J. Jiao, C. Liang, Q. Wang, and X. Zhou, "Calibration of airborne interferometric SAR data based on reference DEM," *Cehui Xuebao/Acta Geodaetica et Cartographica Sinica*, vol. 43, no. 1, pp. 74–82, 2014.

[14] J. Ma, H.-J. You, and D.-H. Hu, "Block adjustment of InSAR images based on the combination of F. Leberl and interferometric models," *J. Infr. Millim. Waves*, vol. 31, no. 3, pp. 271–276, Jun. 2012.

[15] P. H. Chen and I. J. Dowman, "Space intersection from Ers-1 synthetic aperture radar images," *Photogramm. Rec.*, vol. 15, no. 88, pp. 561–573, Oct. 1996.

[16] J. C. Curlander, "Location of spaceborne SAR imagery," *IEEE Trans. Geosci. Remote Sens.*, vol. GE-20, no. 3, pp. 359–364, Jul. 1982.

[17] G. Jin, Y. Wu, M. Xiang, Q. Xu, and Z. Qin, "Baseline estimation algorithm of InSAR with block adjustment," *Acta Geodaetica et Cartographica Sinica*, vol. 40, no. 5, pp. 616–622, 2011.

[18] L. J. Lu and G. M. Huang, "A single-pass airborne interferometric calibration method research for DEM mapping," *Int. Arch. Photogramm., Remote Sens. Spatial Inf. Sci.*, vol. 43, pp. 331–336, Aug. 2020.

[19] J. Gao, Z. Sun, H. Guo, L. Wei, Y. Li, and Q. Xing, "Experimental results of three-dimensional modeling and mapping with airborne Ka-band fixed-baseline InSAR in typical topographies of China," *Remote Sens.*, vol. 14, no. 6, p. 1355, Mar. 2022.

[20] T. Toutin, "Path processing and block adjustment with RADARSAT-1 SAR images," *IEEE Trans. Geosci. Remote Sens.*, vol. 41, no. 10, pp. 2320–2328, Oct. 2003.

[21] S. C. Yang, G. M. Huang, Z. Zhao, and L. J. Lu, "Method of airborne SAR image match integrating multi-information for block adjustment," *Int. Arch. Photogramm., Remote Sens. Spatial Inf. Sci.*, vol. 40, pp. 191–195, Jun. 2015.

[22] X. J. Yue and G. M. Huang, "Multi-photo combined adjustment with airborne SAR images based on a few ground control points," in *Proc. Int. Workshop Earth Observ. Remote Sens. Appl.*, Jun. 2008, p. 314.

[23] J. Ma, H.-J. You, H. Long, and C.-B. Ding, "A new method of block adjustment of airborne SAR images with few GCPs," *J. Electron. Inf. Technol.*, vol. 32, no. 12, pp. 2842–2847, Jan. 2011.

[24] M. Yang, M. Liao, Q. Xiaoqiong, and X. Shi, "Analysis of capabilities of C-and L-band SAR data to detect newly-reclaimed area," *Geomatics Inf. Sci. Wuhan Univ.*, vol. 42, no. 9, pp. 1300–1305, 2017.

[25] Y. Chang, Q. Xu, X. Xiong, G. Jin, H. Hou, and R. Cui, "A robust method for block adjustment of UAV SAR images," *IEEE Access*, vol. 11, pp. 43975–43984, 2023.

[26] L. C. Graham, "Synthetic interferometer radar for topographic mapping," *Proc. IEEE*, vol. 62, no. 6, pp. 763–768, Jun. 1974.
[27] G. Jin, X. Xiong, Q. Xu, Z. Gong, and Y. Zhou, "Baseline estimation algorithm with block adjustment for multi-pass dual-antenna InSAR," *Int. Arch. Photogramm. Remote Sens. Spatial Inf. Sci.*, vol. 41, pp. 39–45, Jun. 2016.
[28] F. Dellinger, J. Delon, Y. Gousseau, J. Michel, and F. Tupin, "SAR-SIFT: A SIFT-like algorithm for SAR images," *IEEE Trans. Geosci. Remote Sens.*, vol. 53, no. 1, pp. 453–466, Jan. 2015.
[29] S. Wei, S. Zhong-Ping, Z. Dongling, S. Chong-Li, Z. Chao, and Y. Jian-Yu, "Hierarchical moving curved fitting filtering method based on LiDAR data," *Nat. Remote Sens. Bull.*, vol. 13, no. 5, pp. 827–839, 2009.
[30] N. Wang, "Research on airborne InSAR DEM block adjustment with independent model," M.S. thesis, Chin. Acad. Surveying Mapping, Beijing, China, 2011.

HAO ZHANG received the B.S. and M.S. degrees from the Institute of Geospatial Information, Information Engineering University, Zhengzhou, China, in 2012 and 2015, respectively. He is currently pursuing the Ph.D. degree with Information Engineering University.

He is a Research Associate with the Xi'an Research Institute of Surveying and Mapping. His research interests include radargrammetry and synthetic aperture radar interferometry.

GUOWANG JIN received the B.S., M.S., and Ph.D. degrees in photogrammetry and remote sensing from the Institute of Geospatial Information, Information Engineering University, Zhengzhou, China, in 2000, 2003, and 2007, respectively.

He is currently a Professor and a Ph.D. Supervisor with Information Engineering University. His research interests include radargrammetry and synthetic aperture radar (SAR) interferometry.

XIN XIONG received the B.S., M.S., and Ph.D. degrees in photogrammetry and remote sensing from the Institute of Geospatial Information, Information Engineering University, Zhengzhou, China, in 2014, 2017, and 2021, respectively.

He is currently a Lecturer with Information Engineering University. His research interests include image feature extraction and matching.

JIN WANG received the B.S. degree in remote sensing science and technology from Chang'an University, Xi'an, in 2010, and the M.S. and Ph.D. degrees in photogrammetry and remote sensing from Wuhan University, Wuhan, in 2012 and 2018, respectively.

Since 2020, he has been a Postdoctoral Fellow with the School of Surveying and Mapping, PLA Strategic Support Force, Information Engineering University. His research interests include joint adjustment of spaceborne laser data and optical satellite imagery and polar remote sensing.

KAI GUAN received the B.S. degree from the University of Science and Technology, Nanjing, China, in 2014, and the M.S. degree from Information Engineering University, Zhengzhou, China, in 2021.

He is currently an Engineer with the Xi'an Surveying and Mapping Station. His research interests include radargrammetry and computer vision.